EFPI-FBG hybrid sensor for simultaneous measurement of high temperature and large strain

Li Xiong (熊 丽)[1,2,3*], Dongsheng Zhang (张东生)[1,3], Litong Li (李立彤)[1,3], and Yongxing Guo (郭永兴)[4]

[1]*National Engineering Laboratory for Fiber Optic Sensing Technology, Wuhan University of Technology, Wuhan 430070, China*

[2]*School of Mechanical and Electronic Engineering, Wuhan University of Technology, Wuhan 430070, China*

[3]*Key Laboratory of Fiber Optic Sensing Technology and Information Processing, Ministry of Education, Wuhan University of Technology, Wuhan 430070, China*

[4]*School of Machinery and Automation, Wuhan University of Science and Technology, Wuhan 430081, China*

[*]*Corresponding author: xiong_tuotuo@163.com*

Received August 6, 2014; accepted October 11, 2014; posted online November 28, 2014

We report an extrinsic Fabry–Perot interferometer-fiber Bragg grating (EFPI-FBG) hybrid sensor in this letter. The interferometric cavity of the proposed hybrid sensor is composed of a glass capillary tube, a section of single-mode fiber, and a section of single-mode metal fiber with one FBG. The FBG processed by high-temperature annealing is used to measure temperature, whereas the fiber EFPI is adopted for strain measurement. One of the two aligned fibers is free along the axial direction, which is different from the traditional structure that both the fibers are fixed to glass capillary tube. Experimental results show that the sensor can measure high temperature and large strain simultaneously. The measuring range of temperature and strain for the hybrid sensor is up to 500 °C and 10,000 $\mu\varepsilon$, respectively. Effective temperature compensation of the hybrid sensor is realized, too.

OCIS codes: 060.2300, 060.2370.
doi:10.388/COL201412.120605.

Optical fiber sensors have received great attention by various researchers owing to its prominent advantages such as small profile, light weight, high precision, and immunity to electromagnetic interference and high resistance to corrosive environments[1–4]. Among all the fiber-optic sensors, fiber Bragg grating (FBG) and extrinsic Fabry–Perot interferometer (EFPI) sensors are wavelength encoded, which overcome the negative influence caused by the fluctuation of light source. Varieties of FBG and EFPI sensors have been designed and used in hostile environment, such as downhole application, large concrete and masonry structures, and chemical and medicine sensing[5–7]. Multi-parameter monitoring is a wide topic in fiber sensing area because of its miniature size, less complexity, and low cost. Also the problem of parameter discrimination is solved where cross-sensitivity is an important issue[8].

In recent years, many approaches have been reported for simultaneous strain and temperature measurement based on fiber grating and Fabry–Perot (FP) interferometry. Rao *et al.* developed an EFPI-FBG integrated sensor for simultaneous measurement of strain and temperature[9]. In their work, the EFPI was fabricated by inserting two single-mode fibers with cleaved ends into a glass capillary tube and the cavity length of FP was the air gap between the two faces of the cleaved fibers. The fibers were then fixed to the glass capillary tube using epoxies. This sensor was tested only under a temperature range of 25–85 °C and a strain range of 0–1600 $\mu\varepsilon$, which obtained an accuracy of 1 °C and 20 $\mu\varepsilon$. Because of the creeping property of epoxy and the different coefficients of thermal expansion (CTEs) of epoxies, glass tubes, and fibers, the sensor is cross-sensitive to temperature and strain. Thus, big error may occur in simultaneous strain and temperature measurement. Besides that, some other new approaches have been reported in the field of simultaneous strain and temperature measurement. A combined long-period fiber grating (LPFG) and FP sensor was proposed by Liao *et al.*[10]. The sensor was fabricated by laser pulses and LPFG was used for high-temperature measurement, which made the sensor measure a strain of 500 $\mu\varepsilon$ under a high-temperature environment of 500 °C. These functions were also measured by other sensors, such as laser-machined cascaded microcavities[11], PCF-based FP interferometric sensor[12], and FBG/FP integrated sensor-based etching method[13]. All these sensors have some common characteristics: simple and novel structures, simultaneous measurement of dual parameters (strain and temperature), and consider temperature compensation during measurement. But, these sensors are fabricated using a similar mode in which two fibers are bonded together by fusion splicing. In this mode, solder joint is the delicate part of the whole sensor which limits large-strain measurement of the sensor. In general, these sensors reported before

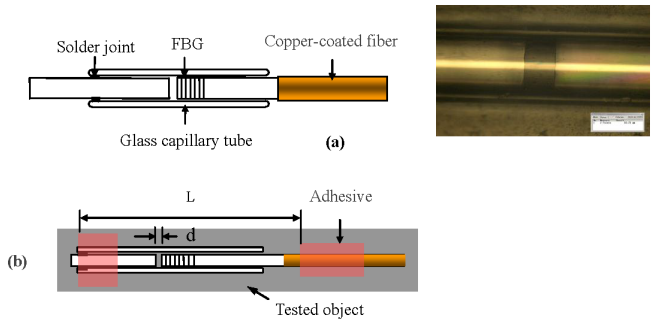

Fig. 1. (a) Configuration and photograph of the EFPI/FBG hybrid sensor and (b) schematic diagram of the hybrid sensor coupled to an object.

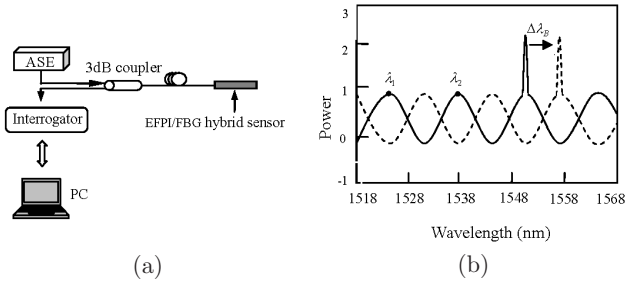

Fig. 2. Schematic of demodulation principle: (a) white light interferometer system and (b) reflective spectrum for EFPI/FBG.

can measure high temperature, even 1000 °C, but the measuring range of strain is mainly less than 3000 $\mu\varepsilon$.

We present a novel EFPI-FBG hybrid sensor fabrication where the excellent temperature resistance of annealed Bragg grating[14] and copper-coated metal fiber[15] makes the sensor measure high temperature. Electrical discharge welding is done just on one side of the sensor, whereas the other fiber can slide freely along the axial direction of the glass capillary tube. During the measurement, the glass capillary tube and the free fiber are fixed to the object to be detected. In this structure, there is no force acted on the sensor, which allows the sensor measure large strain. Furthermore, the FBG is used for temperature measurement, which is used to compensate the strain measurement error caused by temperature–strain cross-sensitivity.

The structure of the EFPI-FBG hybrid sensor is shown in Fig. 1(a). The EFPI sensor is fabricated by inserting two single-mode optical fibers (Φ125 μm) with clean and flat ends into a glass capillary tube with an inner diameter of 128 μm. The clean and flat ends are obtained by optical grinding and cutting. The FP cavity length is the air gap between the two ends of the fibers. On the right side of the sensor, we use a copper-coated metal fiber to guide the light transmission and a FBG is written on the top of the fiber. The FBG is annealed under 550 °C, which endows it a high-temperature resistance. The FBG was fabricated in laboratory using phase mask technology. A KrF excimer laser beam (248 nm) was modulated spatially using a phase mask grating. The main purpose of using the copper-coated metal fiber is to protect the fiber out of the glass capillary tube. The fabrication of copper-coated metal fiber is already reported by our group[15]. The fabrication process of metal-coated fiber is as follows: a Cr film with a thickness of 20 nm is coated on a single-mode optical fiber by magnetron sputtering to form good adhesion toward the surface of optic fiber. And then, the Cr film is covered with an Ag film (approximately 40 nm) for excellent electrical conductivity. Finally, a cuprum film is electroplated onto the surface of the Ag film. The copper-coated metal fiber and the annealed FBG are designed for better resistance to high temperature. The copper-coated metal fiber can slide freely along the axial direction of the capillary glass tube before fixing it. A photograph of the assembled hybrid sensor is presented in Fig. 1(a).

The fabricated sensor is coupled to the object to be detected as shown in Fig. 1(b). High-temperature resistant inorganic adhesive is used to couple the glass capillary tube and the metal fiber to the detected object. The key physical dimensions d and L as shown in Fig. 1 are the optic path difference (OPD) of the sensor and the effective measured length, respectively. When the detected object expands with heat, the sensor will have a microdisplacement with the object. During the construction of the integrated sensors, an interrogator based on white light demodulation principle is used to interrogate the reflective spectra of the compound signal due to the FP interferometer and FBG reflection. As shown in Fig. 2(a), light beam from the ASE is transmitted through the coupler to the EFPI-FBG sensor. Light interference is formed between the two ends of the air cavity of the EFPI and then reflected to the demodulation module of the interrogator. The interrogator receives the reflected compound spectrum. Then the reflected EFPI/FBG spectrum is analyzed using LabVIEW. The EFPI/FBG wavelength data are recorded by a high-speed home-made FBG interrogator with an acquisition rate of 2 kHz, and an accuracy of 1 pm.

The reflective spectrum for hybrid sensor based on EFPI and FBG is shown in Fig. 2(b). The strong narrowband peak is the signal from FBG. As the strain and temperature change, the wavelength of the FBG and the spectrum of the EFPI shift, which helps to calculate the variation in parameters.

(1) Temperature measurement

Correlation method to detect the FBG wavelength shift[16] is

$$\mathrm{ccf}(k\cdot \mathrm{d}\lambda) = \sum_{i=0}^{M-1} R_1(i,\mathrm{d}\lambda).R_2\left[(k+i)\mathrm{d}\lambda\right], \qquad (1)$$

where ccf is a discrete cross-correlation coefficient, which is obtained by a spectral increment of the FBG reference spectrum $k\bullet \mathrm{d}\lambda$ (k = 0, ±1, ±2, …), i…M and $\mathrm{d}\lambda$ are the sampling points and spectral resolution,

respectively, and R_1 and R_2 are the reflected EFPI/FBG spectrum and the known FBG reference spectrum, respectively. A spectral increment of k in R_2 is equal to the shift of the wavelength in R_1. This amplitude of the cross-correlation measures the maximum value, which is used to detect the shift of the Bragg wavelength $\Delta\lambda_B$.

With ΔT being the variation of temperature and λ_B the center wavelength of FBG, the temperature measuring principle of FBGs is

$$\frac{\Delta\lambda_B}{\lambda_B} = (\xi + \alpha) \times \Delta T, \tag{2}$$

where α and ξ are the CTE and thermo-optical coefficient, respectively. That is

$$\Delta\lambda_B = k \times \Delta T, \tag{3}$$

where $k=(\alpha+\xi)\times\lambda_B$ is the temperature coefficient, which is obtained from the temperature calibration experiment.

(2) Strain measurement

By tracing the peak points in the interference spectrum, the air gap value of the sensor was demodulated. The EFPI cavity length d was calculated from the reflected spectrum as

$$d = \frac{\Delta\varphi \cdot \lambda_1\lambda_2}{4\pi(\lambda_2 - \lambda_1)}, \tag{4}$$

where $\Delta\varphi$ is the phase difference of two wavelengths λ_1 and λ_2. λ_1 and λ_2 are adjacent peak points in the reflected spectrum (Fig. 2(b)). We can infer that $\Delta\varphi = 2\pi$. Thus, Eq. (4) can be simplified as

$$d = \frac{\lambda_1\lambda_2}{2(\lambda_2 - \lambda_1)}. \tag{5}$$

Thus, the strain is determined by calculating the variation in the cavity length Δd

$$\varepsilon = \frac{\Delta d}{L}. \tag{6}$$

A schematic of the experimental set-up is shown in Fig. 3. The object to be tested was fixed on a two-dimensional translation stage (1 μm resolution at X and Y directions). An EFPI-FBG hybrid sensor was encapsulated on the upper surface of the object, whereas a commercially available absolute strain sensor was fixed on the lower surface which was used as a reference strain sensor. Readings from the reference sensor were acquired using a date acquisition system (DAQ). A heat source was employed to heat up the object along with a thermo detector to monitor the experimental temperature which acts as the reference temperature.

The strain sensing property of the sensor was tested at constant room temperature (room temperature). Mechanical strain was applied to the sensor by turning the knob of the translation stage along the axial direction. During the test, the strain applied to the tested object was measured by the EFPI/FBG hybrid sensor

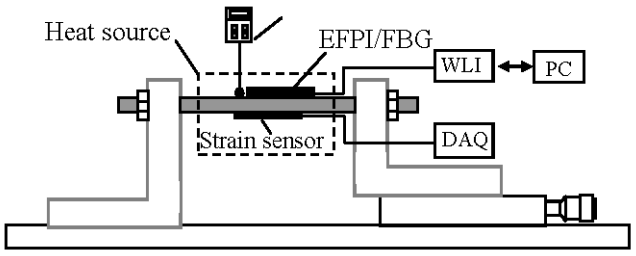

Fig. 3. Experimental setup.

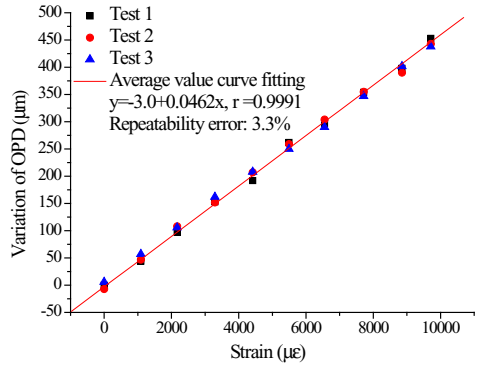

(a)

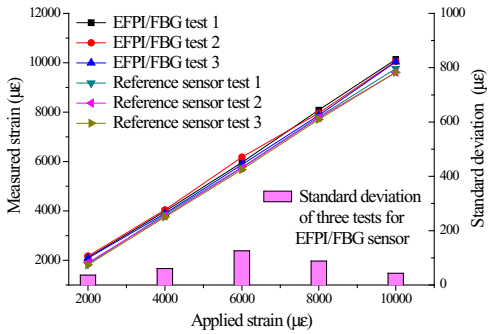

(b)

Fig. 4. Strain performance of hybrid sensor: (a) strain response for EFPI and (b) correlation between measured strain and applied strain.

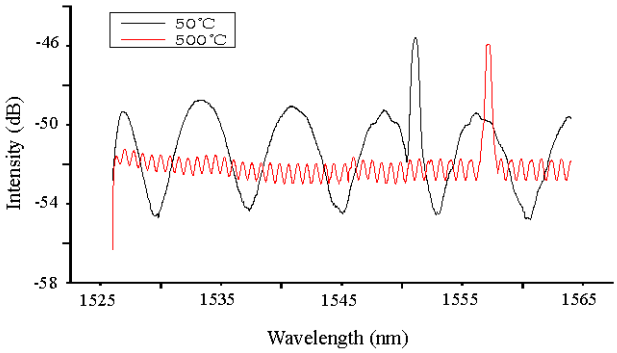

Fig. 5 Reflection spectra under different temperatures.

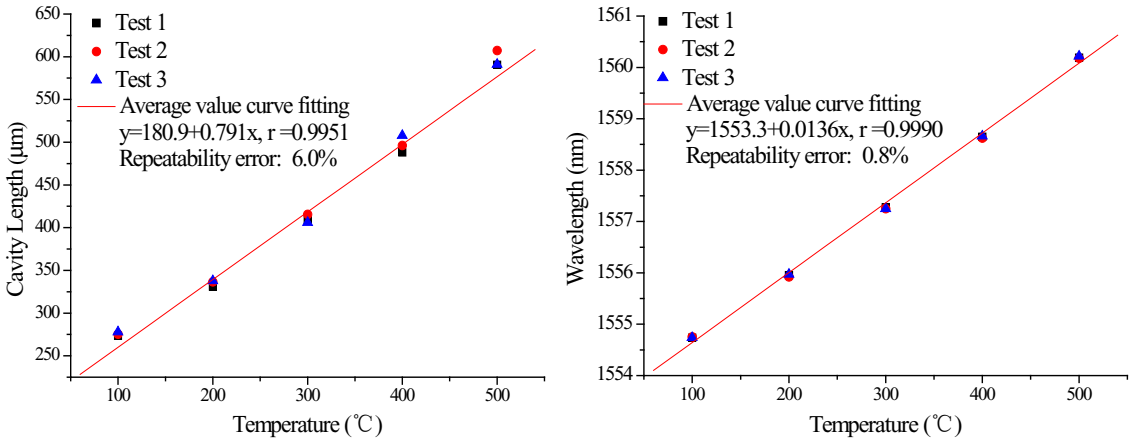

(a) Temperature response for EFPI (b) Temperature response for FBG

Fig. 6. Temperature performance of hybrid sensor.

and the reference sensor, simultaneously. The test is repeated three times. Figure 4(a) shows that a sensitivity of 46 nm/$\mu\varepsilon$ is achieved with excellent linearity of 0.9991 and repeatability of 3.3% to strain. Moreover, a comparison of measuring results between the EFPI/FBG hybrid sensor and the reference sensor is presented in Fig. 4(b), which demonstrates a good consistency. The standard deviation of three tests for the EFPI/FBG sensor is also plotted in Fig. 4(b). This strain test demonstrates the measurement of large strain (10000 $\mu\varepsilon$) using the EFPI/FBG hybrid sensor.

Temperature characterization was investigated under the condition of no strain to the object. Temperature measurements were done at room temperature with an increment of 100 up to 500 °C. The test is repeated three times. Figure 5 shows the reflection spectra under different temperatures. Figure 6 shows the temperature sensitivity of the sensor.

The reflective spectra of the sensor at 50 and 500 °C are shown in Fig. 5, which indicates that the reflective spectra of FBG and EFPI shift via temperature simultaneously. The cavity length of the sensor increased constantly when the test object expanded with heat, which makes the interference fringes of the reflective spectrum of EFPI become denser in quantity and weaker in intensity, whereas the intensity of the spectrum of FBG remains the same because of high-temperature annealing. As shown in Fig. 6, when the temperature changes from room temperature to 500 °C, a temperature sensitivity of 13.6 pm/°C with a repeatability error of 0.8% for FBG wavelength and 0.79 μm/°C with a repeatability error of 6.0% for cavity length are obtained, respectively. This sensor has excellent linearity and repeatability to temperature.

From the temperature characterization of the hybrid sensor, we see that temperature variations not only cause wavelength shift of FBG but also change the OPD of EFPI due to thermal expansions of the test object and the sensor itself. (The CTE of SiO_2 is much less than that of metal, so it can be ignored here.) Temperature compensation is essential as a strain error is caused by the temperature cross-sensitivity of the EFPI. In this EFPI/FBG hybrid sensor, the FBG used for temperature measurement was employed for temperature compensation where pure force strain can be separated from total strain by subtracting thermal strain.

The thermal strain could be calculated by

$$\varepsilon_{\mathrm{T}} = \frac{\alpha \cdot l \cdot \Delta T}{l} = \alpha \cdot \Delta T, \tag{7}$$

where α is the CTE of the test object, ΔT is measured by the FBG as shown in Eq. (3) and $\alpha \cdot l \cdot \Delta T$ is the variation of OPD caused by thermal expansion.

Thus, we can acquire the pure force strain ε_s from Eqs. (6) and (7) as

$$\varepsilon_{\mathrm{S}} = \varepsilon - \varepsilon_{\mathrm{T}} = \frac{\Delta d}{l} - \alpha \cdot \Delta T. \tag{8}$$

Thus, temperature cross-sensitivity of the sensor can be eliminated.

During the test, the temperature was changed randomly from 250 to 360 °C. Three actual strains of 700, 1400, and 1800 $\mu\varepsilon$ have been applied on the sensor successively and each strain load is kept for 2 min. Figure 7 shows

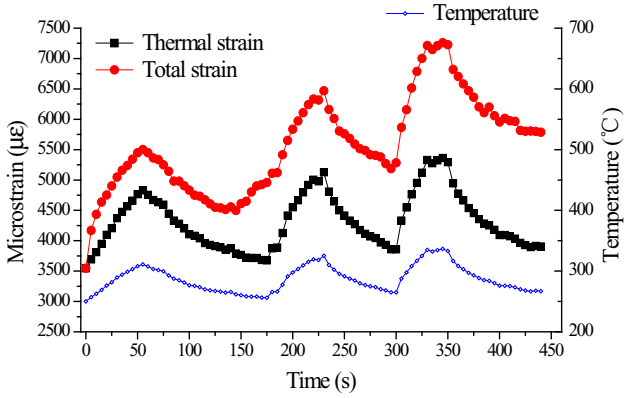

Fig. 7. Real-time curves of the total strain and thermal strain measured by the sensor.

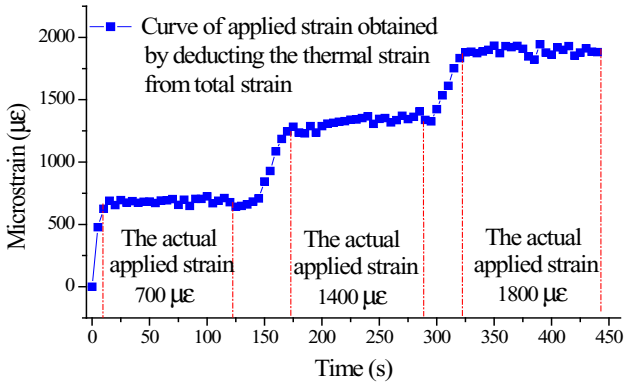

Fig. 8. Applied strain measured by the EFPI/FBG sensor.

the real-time curves of temperature and strain (including total strain and thermal strain) measured by the sensor. The left *Y*-axis represents microstrain, whereas the right *Y*-axis represents the environment temperature. The applied strain curve can be obtained by subtracting the thermal strain from the total strain. As shown in Fig. 8, the applied strain tendency has been presented effectively, which consists of the actual load.

In conclusion, we investigate the performance of strain and temperature for an EFPI/FBG hybrid sensor, which can measure large-strain and high-temperature measurements. Temperature and strain sensitivities measured by the sensor are 13.6 pm/°C and 46 nm/$\mu\varepsilon$, respectively. The measuring range of temperature and strain are up to 500 °C and 10000 $\mu\varepsilon$, respectively. Moreover, a reasonable temperature compensation method solves the problem of temperature cross-sensitivity.

This work was supported by the National High Technology Research and Development Program under Grant No. 2012AA041203.

References

1. K. Liu, in *Proceedings of IEEE Instrumentation and Measurement Technology Conference* 714 (1997).
2. K. T. V. Grattan and T. Sun, Sens. Actuators **82,** 40 (2000).
3. G. Tang, J. Wei, W. Zhou, R. Fan, M. Wu, and X. Xu, Chin. Opt. Lett. **12,** 090604 (2014).
4. S. Yang, H. Sun, L. Yuan, X. Zhang, L. Zhou, and M. Hu, Chin. Opt. Lett. **11,** 120604 (2013).
5. D. M. McCann and M. C. Forde, NDT&E Int. **34,** 71 (2001).
6. Y. Rao, Opt. Lasers Eng. **31,** 297 (1999).
7. S. H. Aref, H. Latifi, M. I. Zibaii, and M. Afshari, Opt. Commun. **269,** 322 (2007).
8. H. Singh and J. S. Sirkis, J. Lightw. Technol. **15,** 647 (1997).
9. Y. Rao, X. Zeng, Y. Zhu, Y. Wang, T. Zhu, Z. Ran, S. Yuan, and D. Liang, Acta Opt. Sin. **22,** 85 (2002).
10. X. Liao, Y. Rao, Z. Ran, and H. Deng, Chin. J. Laser **35,** 884 (2008).
11. Y. Rao and Z. Ran, Opt. Fiber Technol. **19,** 808 (2013).
12. M. Deng, C. Tang, T. Zhu, and Y. Rao, IEEE Photon. Technol. Lett. **23,** 700 (2011).
13. L. Li, X. L. Tong, C. M. Zhou, H. Q. Wen, D. J. Lv, K. Ling, and C. S. Wen, Opt. Commun. **284,** 1612 (2011).
14. J. Y. Li, "Sensing property and technology research on fiber optic sensing in high and low temperature environment," PhD. Thesis (Wuhan University of Technology, 2013).
15. Y. Guo, D. Zhang, Z. Zhou, L. Xiong, and X. Deng, Chin. Opt. Lett. **11,** 070604 (2013).
16. K. Bremer, E. Lewis, G. Leen, B. Moss, S. Lochmann, and I. Mueller, in *Proceedings of IEEE Conference on Sensors* 105 (2011).